Available online at www.sciencedirect.com
SCIENCE DIRECT®
International Journal of Heat and Mass Transfer 48 (2005) 2360–2371
International Journal of HEAT and MASS TRANSFER
www.elsevier.com/locate/ijhmt

Convective heat transfer characteristics of electro-osmotically generated flow in microtubes at high wall potential

B.C. Liechty, B.W. Webb *, R.D. Maynes

Department of Mechanical Engineering, Brigham Young University, 435L CTB, Provo, UT 84602-4102, USA

Received 6 July 2004; received in revised form 25 January 2005
Available online 21 March 2005

Abstract

Fully-developed convection heat transfer for electro-osmotic flow in a circular microtube has been investigated for arbitrary wall zeta potentials under conditions of imposed wall temperature and imposed wall heat flux. The coupled differential equations governing charge potential, momentum, and energy were solved numerically. It has been determined that elevated values of wall zeta potential produce significant changes in the charge potential, electro-osmotic flow field, temperature profile, and Nusselt number relative to previous results invoking the Debye–Hückel linearization, which is valid only for low wall potentials.

1. Introduction

Fluid transport in microtubes is found in a variety of emerging applications from inkjet printers to biomedical devices. Traditional pressure-based methods of inducing flow in channels of cross-sections less than 100 μm can be prohibitive due to the extraordinarily high pumping pressures required. Further, precise control and stability are often requisite, and are difficult to achieve using traditional technologies. Electro-osmosis offers benefits over conventional pressure-driven flow in microchannels. It represents an efficient, precisely controllable means of driving flow which requires no moving parts. Further, electro-osmotic flow produces velocity profile characteristics which are desirable in a number of applications.

Electro-osmosis is the bulk motion of a fluid due to an applied electric field [1]. When exposed to an ionizing fluid, many solid materials will develop a small electric charge at their surface. This charge will attract ions of opposite charge in the fluid layer adjacent to the solid surface. The result is the formation of a layer of charged ions near the surface called the electric double layer (EDL). Within the EDL there is an excess of charged ions distributed diffusely from a maximum concentration very near the solid surface, termed the wall or zeta potential, ζ_w, to a neutral charge state in the core fluid far from the surface. Typical wall potentials range from 30 to 200 mV [2], although it may be possible to tailor the wall potential by imposing voltage gradients in the direction normal to the microchannel axis [3], thus yielding wall potentials in excess of these limits. The thickness of the EDL is characterized by the Debye length, λ, which defines the distance from the charged solid surface to which the charge drops to e^{-1} (37%) of its maximum. The Debye length is a function of the electro-chemistry of the liquid–solid combination, and can range from a

* Corresponding author. Tel.: +1 801 422 6543; fax: +1 801 422 0516.
E-mail address: webb@byu.edu (B.W. Webb).

0017-9310/$ - see front matter © 2005 Elsevier Ltd. All rights reserved.
doi:10.1016/j.ijheatmasstransfer.2005.01.019

Nomenclature

a	tube radius
c	fluid specific heat
c_0	concentration of ions in bulk fluid
E_e	normalized ratio of total Joule heating per unit tube length, Eq. (15)
$\overline{E}_e$	total Joule heating per unit tube length, Eq. (14)
E_x	imposed axial potential gradient
h	convective heat transfer coefficient
i_e	conduction current density
k	fluid thermal conductivity
Nu	Nusselt number, $h(2a)/k$
r	radial coordinate
R	normalized radial coordinate, r/a
R_u	universal gas constant
q''_w	wall heat flux
S	Joule heating parameter, $E_x^2 a/\sigma q''_w$
S_T	Joule heating parameter yielding a constant wall temperature condition, Eq. (16)
T	local absolute temperature
T_m	mixed mean temperature
T_w	tube wall temperature
u	local fluid velocity
u_{eo}	maximum possible electro-osmotic velocity, $(\varepsilon\zeta_w/\mu)E_x$
$\bar{u}$	average velocity
U	normalized local velocity u/u_{eo}
$\overline{U}$	ratio of mean velocity to maximum electro-osmotic velocity, $\bar{u}/u_{eo}$
x	streamwise coordinate
$z_\pm$	valence number of the positive/negative ions in solution
z_e	valence number of the univalent solution
Z	electro-kinetic radius, a/λ

Greek symbols

α	fluid thermal diffusivity
ε	fluid permittivity
λ	Debye length, $(\varepsilon R_u T/2z_e^2 F^2 c_0)^{1/2}$
μ	fluid absolute viscosity
ρ_e	local charge density
σ	fluid electrical resistivity
θ	normalized temperature, $(T - T_m)/(q''_w a/k)$
θ_w	normalized wall temperature, $(T_w - T_m)/(q''_w a/k)$
ψ	local charge potential
Ψ	dimensionless charge potential, $z_e F\psi/R_u T$
ζ_w	wall zeta potential

few nanometers to as high as 1 μm. Higher ion concentrations (resulting, for example, from increased dissolved solute) decrease the Debye length. Electro-osmotic flow occurs when the charged ions in the EDL respond to an externally applied electric field. Charged ions in the EDL are attracted to the oppositely charged electrode, and their movement induces fluid flow by viscous drag. In microchannels, viscous shear transmits these body forces in the EDL to the channel core where little/no electro-kinetic body force exists, pulling the fluid toward the electrode. When the Debye length is small compared to the microtube dimension the momentum body force is confined to a small region near the tube wall, and the resulting velocity profile is uniformly flat. If, on the other hand, the Debye length is of the same order as the microtube dimension, the body force is more uniformly distributed across the tube cross-section and the velocity profile resembles that of a traditional pressure-driven flow. Thus, the ratio of channel radius to Debye length, sometimes termed the electro-kinetic radius, is a key parameter in characterizing the hydrodynamic behavior of electro-osmotic flow. Typical velocities in electro-osmotic flow in microtubes are of the order of a few mm/s.

A considerable body of work in the literature has reported on electro-osmotically generated flow in microtubes. The hydrodynamic problem has received considerable recent attention, with analytical/numerical investigations exploring electro-osmotic flow in a number of geometric configurations [4–10]. This has been accompanied by significant recent effort in developing and exercising experimental techniques for characterizing the electro-osmotic flow in microchannels [11–16]. The characteristics of hydrodynamically developing electro-osmotic flow have also been studied [17,18], as has the influence of variations in fluid and surface properties [19–22].

Prior work characterizing the convective heat transfer in electro-osmotic flow is less abundant. Since the body force is strongly coupled to the charge distribution in the microchannel, the velocity profiles resulting from electro-osmotically generated flow differ dramatically from that of classical pressure-driven flow. Further, the applied voltage gradient results in the passage of electrical current through the fluid column, resulting in Joule heating. The combination of unique velocity profiles and Joule heating yield temperature distributions and associated heat transfer characteristics which are quite unlike those of pressure-driven flow. There has been considerable work seeking to explore Joule heating effects in electro-osmotic flow [23–30]. However, the

focus of these studies has been the fluid heating and the possible degradation in capillary electrophoresis performance, and they therefore have not explored the convective heat transfer in such flows. Some early work explored the general effect of volumetric energy dissipation on the thermal development in channels under pressure-driven flow conditions [31–33].

Recently, analytical solutions for the fully-developed temperature distributions and Nusselt number were presented for fully-developed electro-osmotic flow in parallel plate and cylindrical microchannels at low wall potential [34]. The analysis was subsequently extended to include the influence of viscous heating [35]. An analytical solution for the thermally developing temperature distribution for electro-osmotic flow in rectangular microchannels under the infinitely thin Debye layer assumption was also presented [36]. These heat transfer studies, however, have employed the Debye–Hückel approximation, in which a linearization of the charge distribution is invoked. This assumption restricts the wall potential to less than 20–25 mV [1]. The Debye–Hückel approximation yields a linear dependence of the momentum body force on charge potential in the fluid, and Joule heating which is unrealistically uniformly distributed over the microtube cross-section. In most applications, however, the wall potential is much higher than the Debye–Hückel linearization would allow. This paper reports solutions for hydrodynamically and thermally developed electro-osmotic transport in cylindrical microtubes at arbitrary wall potentials. Analytical solutions for velocity and temperature profiles at realistic values of wall zeta potential are not feasible, and recourse is therefore taken to numerical methods.

2. Analysis

Consider steady-state, hydrodynamically and thermally fully-developed electro-osmotic flow of a fluid in a cylindrical tube of radius a. Temperature differences are assumed to be small, with associated negligible temperature-dependence of the electrical and thermophysical properties. The radial distribution of charge potential, ψ, in the microtube is governed by the Poisson equation [1]

$$\frac{\varepsilon}{r}\frac{\mathrm{d}}{\mathrm{d}r}\left(r\frac{\mathrm{d}\psi}{\mathrm{d}r}\right)=\rho_{\mathrm{e}} \tag{1}$$

where ε is the (constant) permittivity of the fluid, and ρ_{e} is the local charge density. Assuming the solution is in thermodynamic equilibrium, the charge density is related to the charge potential by the Boltzmann distribution [1] as

$$\rho_{\mathrm{e}}=Fc_0z_-\exp\left(z_-F\psi/R_{\mathrm{u}}T\right)-Fc_0z_+\exp\left(z_+F\psi/R_{\mathrm{u}}T\right) \tag{2}$$

which, assuming a symmetric electrolyte of valence number z_{e} may be cast in the form

$$\rho_{\mathrm{e}}=2z_{\mathrm{e}}Fc_0\sinh\left(\frac{z_{\mathrm{e}}F}{R_{\mathrm{u}}T}\psi\right) \tag{3}$$

F is Faraday's constant, R_{u} is the universal gas constant, c_0 is the concentration of ions in the bulk flow, and T is the absolute temperature. In the Debye–Hückel linearization, valid only at low wall potentials (and consequently, low ψ), the assumption is justifiably made that $\sinh(z_{\mathrm{e}}F\psi/R_{\mathrm{u}}T)\approx z_{\mathrm{e}}F\psi/R_{\mathrm{u}}T$ [1]. In this study arbitrary wall potentials are considered, and the non-linear form of the Boltzmann equation source is retained. Boundary conditions associated with Eq. (1) are symmetry at the tube centerline and known zeta potential at the wall. Defining a dimensionless radius and charge potential, respectively, as $R=r/a$ and $\Psi=z_{\mathrm{e}}F\psi/R_{\mathrm{u}}T$, Eq. (1) becomes

$$\frac{1}{R}\frac{\mathrm{d}}{\mathrm{d}R}\left(R\frac{\mathrm{d}\Psi}{\mathrm{d}R}\right)=Z^2\sinh(\Psi) \tag{4}$$

Here, Z is the electro-kinetic radius of the system, defined as the ratio of the microtube radius to Debye length, $Z=a/\lambda$ The Debye length is defined as $\lambda=(\varepsilon R_{\mathrm{u}}T/2z_{\mathrm{e}}^2F^2c_0)^{1/2}$. Boundary conditions for the charge potential are

$$R=0:\quad \frac{\mathrm{d}\Psi}{\mathrm{d}R}=0 \tag{5a}$$

and

$$R=1:\quad \Psi=\Psi_{\mathrm{w}}=(z_{\mathrm{e}}F\zeta_{\mathrm{w}}/R_{\mathrm{u}}T) \tag{5b}$$

The velocity profile is governed by the streamwise differential momentum equation, which, in the absence of applied pressure gradients becomes

$$\frac{\mu}{r}\frac{\mathrm{d}}{\mathrm{d}r}\left(r\frac{\mathrm{d}u}{\mathrm{d}r}\right)=-\rho_{\mathrm{e}}E_x \tag{6}$$

μ is the fluid viscosity and E_x is the applied voltage potential gradient along the axis of the microtube. Note that the charge density, and hence the charge potential, appears in the source term for fluid momentum, thus coupling the governing equations for charge potential and momentum. The body force inducing electro-osmotic flow exists only in regions of non-zero charge potential. One may define a dimensionless velocity as $U=u/u_{\mathrm{eo}}$, where $u_{\mathrm{eo}}=(\varepsilon\zeta_{\mathrm{w}}/\mu)E_x$ is the maximum possible electro-osmotic velocity. At high electro-kinetic radius Z, the velocity profile is radially uniform with a magnitude u_{eo}. This is the classical Helmholz–Schmolukowski condition [1]. The grouping $\varepsilon\zeta_{\mathrm{w}}/\mu$ is often termed the electro-osmotic mobility of the fluid. With this normalization the momentum equation may be written in non-dimensional form as

$$\frac{1}{R}\frac{\mathrm{d}}{\mathrm{d}R}\left(R\frac{\mathrm{d}U}{\mathrm{d}R}\right)=-\frac{Z^2}{\Psi_{\mathrm{w}}}\sinh(\Psi) \tag{7}$$

with associated symmetry and no-slip boundary conditions at the microtube centerline and wall, respectively:

$$R = 0: \quad \frac{dU}{dR} = 0 \tag{8a}$$

$$R = 1: \quad U = 0 \tag{8b}$$

Thermal transport in the flow is governed by the differential energy equation, written as

$$\rho c u \frac{\partial T}{\partial x} = \frac{k}{r}\frac{\partial}{\partial r}\left(r\frac{\partial T}{\partial r}\right) + i_e^2\sigma \tag{9}$$

The last term on the right-hand side of Eq. (9) represents the Joule heating source term, with i_e and σ being the local current density and fluid electrical resistivity, respectively. The current density is related to the charge potential by the relation

$$i_e = \frac{E_x}{\sigma}\cosh\left(\frac{z_e F}{R_u T}\psi\right) \tag{10}$$

The current density and hence, Joule heating source term in the energy equation, depend on the local charge potential ψ. It is noted that viscous heating has been neglected in Eq. (9). For low wall potentials, it has been shown that viscous heating is non-negligible in electro-osmotic flow only in nanoscale channels [35]. It will be shown herein that increases in the wall potential result in a significant increase in the magnitude of the Joule heating, and thus, the viscous heating influence is inconsequential. For an imposed constant heat flux at the wall, q''_w, a thermally fully-developed condition exists where the gradient of local temperature in the streamwise direction is constant and equal in magnitude to the mean temperature gradient, $\partial T/\partial x = dT_m/dx = \text{constant}$. The streamwise gradient in mean temperature is determined from an overall energy balance on the fluid:

$$\rho c \bar{u} a^2 \frac{dT_m}{dx} = 2q''_w a + 2\int_0^a i_e^2 \sigma r\, dr \tag{11}$$

where $\bar{u}$ is the mean velocity in the microtube. Eq. (11) reveals that the mean temperature rises linearly in the thermally fully-developed regime to accommodate the combined energy input of the imposed wall flux and Joule heating over the channel cross-section. Defining a dimensionless temperature as a normalized difference between the local temperature and mean temperature, $\theta = (T - T_m)/(q''_w a/k)$, and substituting Eqs. (10) and (11) into Eq. (9) yields the dimensionless differential energy equation

$$\frac{1}{R}\frac{d}{dR}\left(R\frac{d\theta}{dR}\right) = 2\frac{U}{\overline{U}}\left[1 + S\int_0^1 \cosh^2(\Psi) R dR\right] - S\cosh^2(\Psi) \tag{12}$$

$\overline{U}$ is the dimensionless mean velocity in the channel, $\overline{U} = \bar{u}/u_{eo}$. It might be noted that in the limiting case of low wall potential, $\cosh^2(\Psi) \to 1$, and the source term due to Joule heating becomes constant and independent of R. Eq. (12) is subject to boundary conditions reflecting symmetry and the imposed wall flux,

$$R = 0: \quad \frac{d\theta}{dR} = 0 \tag{13a}$$

and

$$R = 1: \quad \frac{d\theta}{dR} = 1 \tag{13b}$$

The dimensionless parameter $S = E_x^2 a/\sigma q''_w$ which appears in the normalized energy equation may be interpreted as the relative strengths (ratio) of the volumetric Joule heating in the low-ζ_w limit E_x^2/σ, and the fluid heating due to imposed wall heat flux q''_w/a. Note that the dimensionless Joule heating parameter S may range in magnitude from 0 (for vanishing Joule heating and/or infinite wall flux) to ∞ (for vanishing wall heat flux). Further, a scenario will be identified hereafter for which the Joule heating parameter S may take on a single, negative value for a given electrokinetic radius and dimensionless wall potential. This condition defines a constant wall temperature thermal boundary condition, wherein all energy generated volumetrically in the fluid due to Joule heating is dissipated at the microtube wall, yielding a negative wall heat flux q''_w.

It should be underlined that the analysis presented here has invoked the traditional assumption that the electrical and thermophysical properties are independent of temperature. Of course, these properties do depend on temperature. The dielectric constant of water decreases by approximately 0.5%/°C in the temperature range 20–80 °C [37]. The electrical and thermal conductivities increase by approximately 2–3%/°C and 0.1–0.3%/°C, respectively. The viscosity of water decreases with temperature by 1.2–2.3%/°C [38]. In the most rigorous analysis, Eqs. (3), (6) and (9) are fully coupled through the property dependence on temperature. It should thus be stated that the influence of temperature-dependent properties may be non-negligible, and the effect of such can only be characterized for a specific electro-osmotic flow/heat transfer scenario by solving the fully coupled equations with temperature-dependent properties. Such a solution is possible. However, for the sake of generality in this exploration of the effects of high zeta potential on the convective heat transfer, the analysis focuses on the limiting case of constant properties. The momentum equation, Eq. (7), is thus dependent on the solution to the charge potential equation, Eq. (4), only through Ψ in the electro-osmotic momentum source term. Further, the energy equation, Eq. (12), exhibits only one-way coupling to both momentum and charge potential equations through the distributions of U and Ψ.

Eqs. (4), (7) and (12) constitute differential equations governing the charge, momentum, and energy transport in the microtube. The solution requires specification of the electro-kinetic radius Z, the dimensionless wall potential Ψ_w, and the Joule heating parameter S. For arbitrary values of Ψ_w, the charge potential equation, Eq. (4), is non-linear and must be solved numerically using an iterative approach. Once the dimensionless charge potential distribution is known, Eqs. (7) and (12) are linear but with radius-dependent source terms, and their solution is straightforward. A control volume approach was adopted for the solution of the governing equations [39]. The radial domain is discretized and Eqs. (4), (7) and (12) are each integrated over an arbitrary cell. A suitable assumption for the variation in dependent variables between nodes is then used to evaluate the integrals. Boundary conditions are imposed similarly by integrating the governing differential equations around the boundary cells, and specifying the boundary condition in the evaluation of the integrals. The discretization procedure yields a set of coupled, nominally linear algebraic equations for the dependent variable at all node points. As stated previously, the differential equation for charge potential, Eq. (4), is non-linear and therefore mandates an iterative solution. Since the source term in the charge distribution equation, Eq. (4), depends on charge potential, the source-term linearization procedure outlined by Patankar was used to accelerate convergence [39]. Iterations were carried out until the absolute maximum residual in Ψ (local imbalance in conservation of Ψ at any given cell) was less than 10^{-7}. After the charge potential distribution had been determined, the velocity and temperature fields were solved directly with substitution of the charge potential field in the source terms in Eqs. (7) and (12). The fully-developed Nusselt number was then calculated from its definition, $Nu = h(2a)/k$, which, in dimensionless form may be written $Nu = 2/\theta_w$, where θ_w is the predicted dimensionless wall temperature. Thus, the local charge potential, velocity, temperature, and Nusselt number, respectively, exhibit the functional dependencies $\Psi = \Psi(Z, \Psi_w, R)$, $U = U(Z, \Psi_w, R)$, $\theta = \theta(Z, \Psi_w, S, R)$, and $Nu = Nu(Z, \Psi_w, S)$.

A non-uniform grid was employed to permit placement of nodes in regions of highest gradients. The nodes were deployed using a parabolic relationship between local node number and radial location, with clustering near the microtube wall. An exhaustive grid independence study was carried out to determine the cell resolution required for accurate predictions. Steep gradients in both charge potential and velocity may exist for high values of the electro-kinetic radius Z. Further, the local Joule heating source terms, described by $\cosh^2(\Psi)$, may be extremely high near the microtube wall at high wall potentials. Fig. 1 illustrates the predicted fully-developed Nusselt number as a function of number of cells

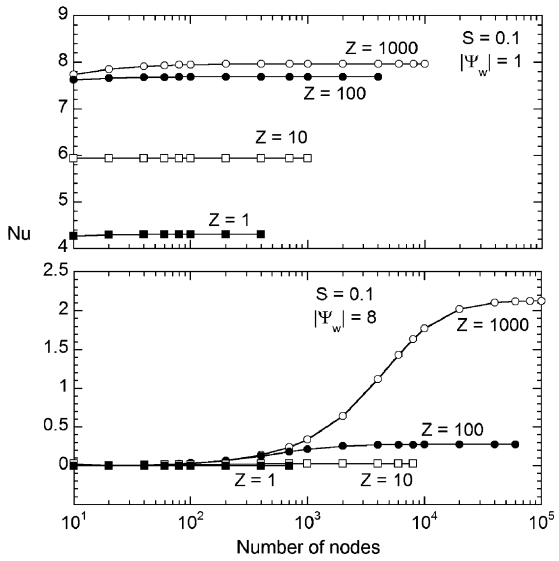

Fig. 1. Illustration of numerical grid refinement required to accurately resolve high gradients in wall potential, electro-osmotic velocity, and Joule heating.

used in the simulation for several different cases. Note that for low Z and Ψ_w, accurate predictions may be achieved with a few tens of cells. Higher Z requires several hundred cells to resolve the high gradients in Ψ and U. At the extreme values of both Z and Ψ_w however, and despite the clustered grid employed, as many as 50,000 nodes are required to adequately resolve the steep charge potential, velocity, and Joule heating source gradients. For all of the simulations presented here, double precision was used in the calculations, and the grid was refined until the predictions for mean velocity and Nusselt number for successively finer grids both ceased to change by more than 1%. Furthermore, numerical predictions from this study for $\Psi_w \to 0$ reproduce the analytical results for Nu of Maynes and Webb [34] over the full range of electro-kinetic radius Z and Joule heating parameter S to within 0.7%.

3. Results and discussion

The predicted normalized charge distribution in the tube is shown in Fig. 2 for electro-kinetic radius $Z = a/\lambda$ of 1, 10, and 100, and for varying absolute dimensionless wall potential, $|\Psi_w| = |z_e F \zeta_w / R_u T|$. The radial variation in charge for arbitrary wall potential has been previously reported [6]. However, these predictions are reproduced here because of their influence on the thermal transport through the local Joule heating, and for completeness. With no external modification of the wall potential through the use of externally applied lateral voltage [3], typical dimensionless wall potentials may

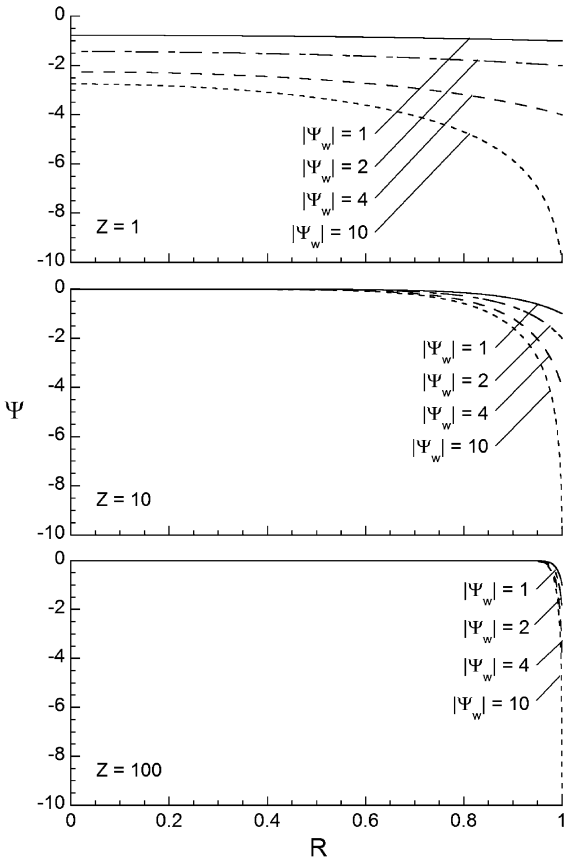

Fig. 2. Radial profiles of dimensionless charge potential as a function of $|\Psi_w|$ and Z.

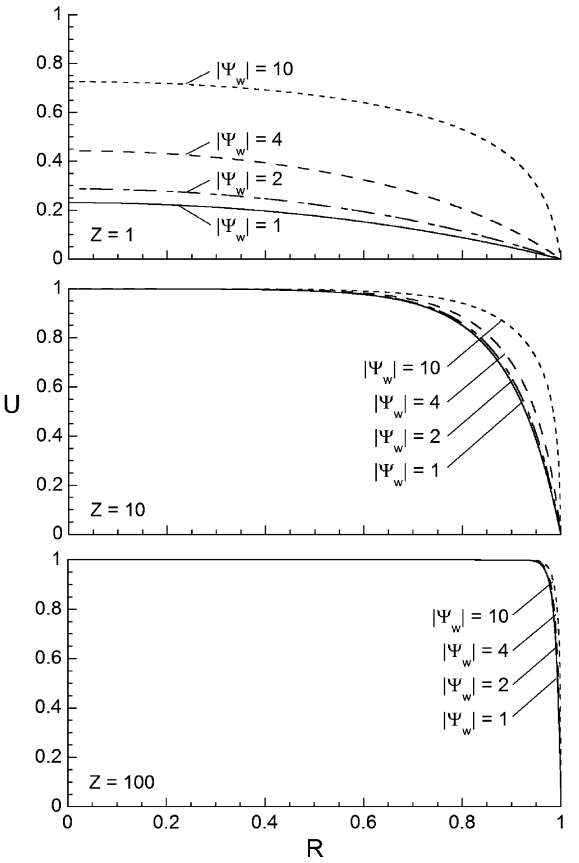

Fig. 3. Radial profiles of the mean electro-osmotic velocity as a function of $|\Psi_w|$ and Z.

vary from 1 to 10 (corresponding to a nominal wall zeta potential magnitude between 25 and 250 mV). The low-wall-potential limit invoked by the Debye–Hückel approximation is traditionally taken to be $|\zeta_w| < 25$ mV ($\Psi_w < 1$). Fig. 2 reveals that for $Z = 1$ the charge potential is distributed diffusely throughout the entire microtube. As Z is increased, a region of non-neutral charge of decreasing size exists near the tube wall. At higher values of Ψ_w the charge potential increases throughout the tube for all values of Z. As Z increases, the EDL is confined to a smaller region near the wall, and increases in Ψ_w have a diminishing influence on the charge profile. Increases in both electro-kinetic radius and the dimensionless wall potential have the same qualitative influence on the transport dynamics.

Since the only driving force in purely electro-osmotic flow is from an electric body force, the charge distribution will significantly influence the electro-osmotic velocity profiles. Recall from Eq. (6) that the local body force in the momentum equation is $\rho_e E_x$, where $\rho_e = 2z_e F c_0 \sinh(z_e F\psi/R_u T)$. Thus, Fig. 2 reveals that a non-zero fluid body force exists in the tube core only for small Z. The source of fluid momentum is located near the tube wall for increasingly large Z and/or large Ψ_w. Fig. 3 illustrates dimensionless velocity profiles in the microtube $U(R)$ for several values of Z and Ψ_w. Again, predictions for electro-osmotic velocity at high wall potential have been previously reported [6], but again, are presented here to highlight their impact on the thermal transport, and for completeness of the study. For the scenario where electro-kinetic forces are present throughout the tube ($Z = 1$), and for low wall potential ($|\Psi_w| = 1$), the velocity profile is nearly parabolic, similar to what would be observed in conventional Poiseuille flow. In this case the body force is distributed more uniformly across the tube cross-section. As $|\Psi_w|$ increases, the velocity magnitude throughout the tube increases, and the velocity profile flattens to some extent, which has qualitatively the same effect as increasing Z. At the other electro-kinetic radius extreme shown ($Z = 100$), the velocity is nearly uniform, and varying Ψ_w has little impact on the hydrodynamics. However, despite the vanishing impact on the velocity profile, it will be shown subsequently that Ψ_w exercises a significant influence on the thermal transport.

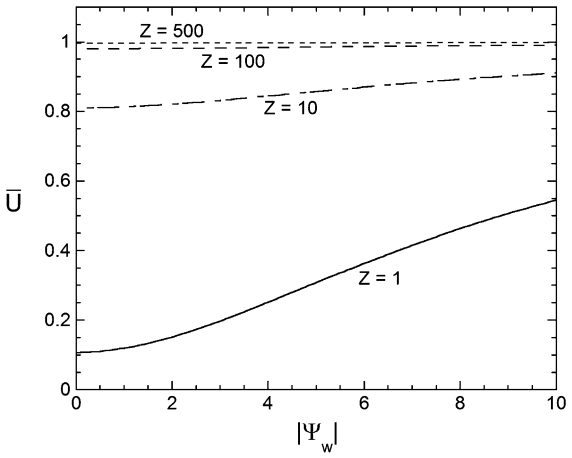

Fig. 4. Variation in dimensionless mean fluid velocity in the microtube as a function of $|\Psi_w|$ and Z.

The dependence of Z and Ψ_w on the mean electro-osmotic flow can be summarized by an investigation of the average fluid velocity in the tube. The normalized average velocity versus Ψ_w is shown in Fig. 4 for values of Z ranging between 1 and 500. Increases in Z beyond 500 yielded negligible changes in $\overline{U}$. At $Z = 1$, the velocity is strongly dependent on Ψ_w, and increasing $|\Psi_w|$ is observed to increase the induced flow. On the other hand, for $Z > 100$, where the flow has reached its maximum possible dimensionless velocity $U = 1 (u = u_{eo})$ throughout nearly the entire channel, the mean velocity exhibits virtually no dependence on Ψ_w.

The predicted flow fields shown in Figs. 3 and 4, and the Joule heating established by the current drawn in the fluid result in thermal transport behavior that is unique to electro-osmosis. The radial variation of the local dimensionless Joule heating source term in the tube, $\cosh^2(\Psi)$, is plotted in Fig. 5 for several values of Z and Ψ_w. For low values of the dimensionless wall potential ($|\Psi_w| < 1$) the volumetric source due to Joule heating is very nearly uniform with a magnitude of unity across the tube for all values of Z. This results from the fact that the electrical current flow in the fluid is distributed nearly uniformly across the tube cross-section for low wall potentials. Increases in the dimensionless wall potential above this low-ζ_w limit results in significant increases in the Joule heating. This occurs primarily near the tube wall for high values of the electro-kinetic radius where the Joule heating may increase by several orders of magnitude in the near-wall region. At low Z (corresponding to large Debye length relative to the tube radius), although the increase in Joule heating is primarily manifest near the wall, large increases across the entire tube are also observed. Fig. 5 illustrates clearly that realistic magnitudes of the wall potential will result in radically different convective heat transfer characteristics than that resulting from an analysis employing the Debye–Hückel approximation (low-ζ_w linearization) [34].

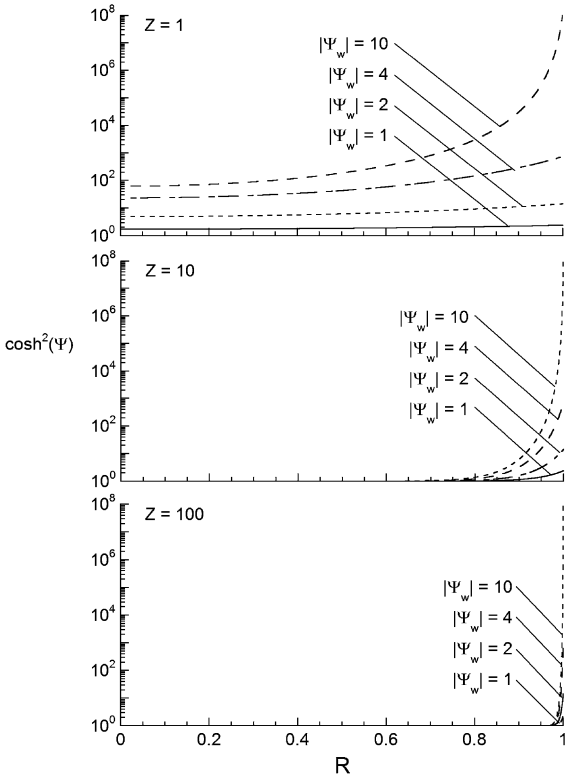

Fig. 5. Radial profiles of the dimensionless Joule heating source in the fluid as a function of $|\Psi_w|$ and Z.

It is instructive to examine the total Joule heating in the fluid per unit microtube length, $\overline{E}_e$. This dimensional quantity is determined by integrating the local Joule heating source term over the cross-section of the tube

$$\overline{E}_e = \int_0^a i_e^2 \sigma 2\pi r \, dr \tag{14}$$

Normalizing this parameter by the total Joule heating per unit length in the low-ζ_w limit $(E_x^2/\sigma)\pi a^2$, the result becomes

$$E_e = \frac{\overline{E}_e}{(E_x^2/\sigma)\pi a^2} = 2\int_0^1 \cosh^2(\Psi) R \, dR \tag{15}$$

Note that E_e is a function of Ψ_w and Z, and is found by integration of the Joule heating source profiles given in Fig. 5. The total dimensionless Joule heating per unit length of the tube E_e is plotted as a function of dimensionless wall potential $|\Psi_w|$ in Fig. 6 for values of Z ranging from 1 to 1000. The behavior reveals that at low wall potential ($|\Psi_w| \to 0$), $E_e \to 1$ for all values of the electro-kinetic radius Z, reflective of the limiting condition where the conduction current is spatially

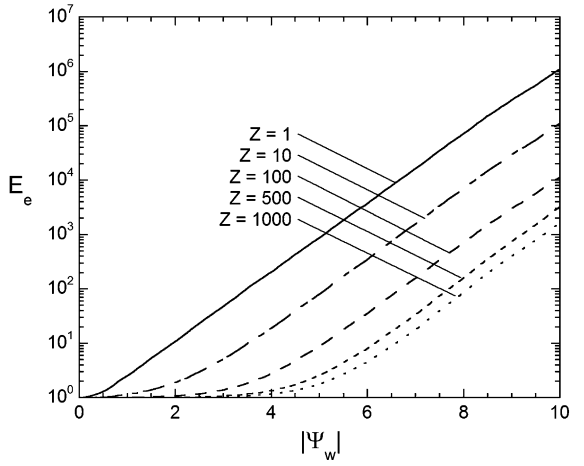

Fig. 6. Normalized Joule heating per unit length of the microtube as a function of $|\Psi_w|$ and Z.

constant in the microtube at the low-ζ_w limit, for which $\cosh^2(\Psi) \to 1$. E_e deviates from this lower bound at increasingly higher dimensionless wall potential as the electro-kinetic radius Z increases. In general, as $|\Psi_w|$ increases so does also the dimensionless total Joule heating, and E_e becomes dependent on Z. For a given value of the wall potential, increases in the electro-kinetic radius yield a reduction in E_e, corresponding to current flow in an ever smaller EDL near the microtube wall. Finally, it is noted that increasing the dimensionless wall potential impacts E_e rather dramatically, where it may increase by as much a six orders of magnitude from the low-ζ_w limit to the highest value of $|\Psi_w|$ investigated, $|\Psi_w| = 10$. For realistic applications utilizing electro-osmotically generated flow, the total Joule heating per unit tube length may easily exceed that predicted by the low-ζ_w limit by several orders of magnitude. This underlines the importance of accounting for realistic values of the wall potential in characterizing the thermal transport.

Attention is now turned to the convective heat transfer in the electro-osmotically generated flow for arbitrary values of the wall potential. The imposed constant wall temperature condition will first be considered, followed by the imposed constant wall heat flux condition.

3.1. Constant wall temperature condition

Recall that S represents the relative strengths of the Joule heating and the imposed wall heat flux, and may vary from zero (for diminishing applied voltage gradient or infinite wall flux) to ∞ (for infinite applied voltage gradient or diminishing wall flux). Although the analysis presented in the foregoing section assumed a uniform heat flux at the microtube wall, the thermally fully-developed condition for a constant wall temperature boundary condition may also be explored. This corresponds to the scenario where all volumetric heating in the fluid is dissipated convectively at the wall, yielding $q''_w < 0$. Thus, the fully-developed condition for imposed constant wall temperature is one of constant wall heat flux as well, where q''_w assumes a particular value which is a function of the total Joule heating. For a given electro-kinetic radius and dimensionless wall potential, there is thus a unique, negative value of the Joule heating parameter (corresponding to fluid cooling) termed here S_T where a constant temperature prevails at the tube wall, and the internal Joule heating is balanced by the imposed (negative) wall heat flux. For this scenario, $dT_m/dx = 0$, and the resulting normalized Eq. (11) yields

$$0 = 1 + S_T \int_0^1 \cosh^2(\Psi) R \, dR \tag{16}$$

Information regarding S_T and its dependence on problem parameters facilitates determination of the unknown wall heat flux for the constant wall temperature condition. Its reciprocal, $1/S_T (= \sigma q''_w / E_x^2 a)$, is a measure of the Joule heating which is dissipated at the wall convectively, normalized by the Joule heating per unit length of microtube for the low-ζ_w limit. Fig. 7 shows values of S_T for a range of Z and $|\Psi_w|$. The figure illustrates that as $|\Psi_w| \to 0$, $S_T \to -2$. This limiting value is in agreement with the analytical solution for the low-ζ_w limit reported previously [34]. As $|\Psi_w|$ increases, however, the magnitude of S_T vanishes. Thus, a significantly higher wall flux is required to dissipate the Joule heating in the fluid, corresponding to a smaller value of $S_T (= E_x^2 a / \sigma q''_w$ for the unique, negative value of q''_w that yields a constant wall temperature boundary).

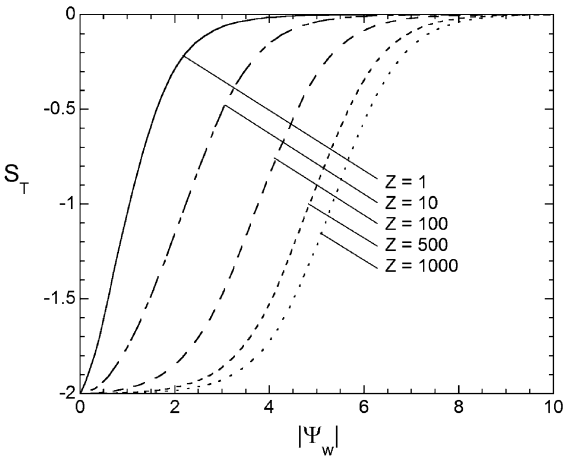

Fig. 7. Variation of the Joule heating parameter yielding a constant microtube wall temperature condition with $|\Psi_w|$ for $1 \leqslant Z \leqslant 1000$.

The variation of S_T with $|\Psi_w|$ shown in Fig. 7 may be correlated with the equation

$$S_T = C_1\{\tanh[C_2(|\Psi_w| - C_3)] - 1\} \quad (17)$$

where C_1, C_2 and C_3 are functions of Z:

$$C_1 = 0.186Z^{-0.536} + 0.993 \quad (18a)$$

$$C_2 = 0.276Z^{-1.95} + 0.743 \quad (18b)$$

$$C_3 = 0.786 + 0.651\ln(Z) \quad (18c)$$

This empirical fit of the predictions yields a peak error of 6% of the maximum S_T ($|S_T|_{max} = 2$), with a typical deviation of approximately 0.5% for the range $1 \leqslant Z \leqslant 1000$ and $0 \leqslant |\Psi_w| \leqslant 10$.

For the constant-temperature boundary condition described here, the magnitude of the wall temperature required to dissipate the total Joule heating, θ_w, is of interest, as it permits calculation of $T_m - T_w$ once the heat flux is known (from S_T). The variation in θ_w is illustrated in Fig. 8 as a function of dimensionless wall potential for a range of electro-kinetic radius. Note that the dependence of θ_w is quite complex, exhibiting a strong dependence on the dimensionless potential. Generally speaking, θ_w increases with increasing $|\Psi_w|$, varying by several orders of magnitude for a given Z. However, the wall temperature is not a monotonic function of Z except in the limit as $|\Psi_w| \to 0$, as was shown previously [34].

3.2. Constant wall heat flux condition

Consider again the scenario involving positive values of S of arbitrary magnitude, for which the imposed wall heat flux results in fluid heating. Figs. 9 and 10 present radial profiles of the dimensionless temperature for several values of Z and Ψ_w at $S = 0.1$ and 10, respectively. Note that for the case of $|\Psi_w| < 1$ an analytical solution for the temperature distribution has been reported [34], and is therefore not shown here. The figures reveal that increases in $|\Psi_w|$ and/or S result in both higher magnitudes and higher radial gradients in θ. For the conditions $S = 0.1$ and $|\Psi_w| = 2$, there is little Joule heating and the dependence of θ on R and Z is rather small. At the other extreme ($S = 10$ and $|\Psi_w| = 10$), the radial variation in θ is dramatic, where even for $Z = 1000$, θ varies radially between −1500 and +1500. Increases in $|\Psi_w|$ have a greater impact on the temperature distribution than increases in S. Changes in S yield nearly proportional changes in θ, whereas variations in Ψ_w result in much more dramatic changes. Larger values of wall potential result in an increase in both the magnitude of the total Joule heating and its radial variation, which generates larger temperature gradients (see Fig. 5). The greatest radial variations in θ are observed for low electro-kinetic radius, Z. This observation is explained by the greater local Joule heating in the central core of the tube at low Z. Generally speaking, as Z increases,

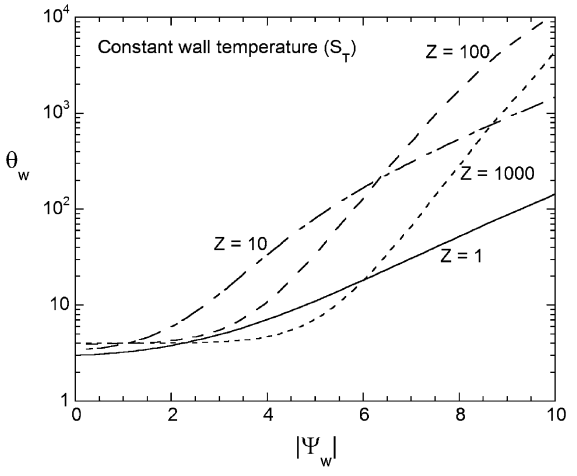

Fig. 8. Dimensionless wall temperature as a function of $|\Psi_w|$ and Z for the constant wall temperature condition.

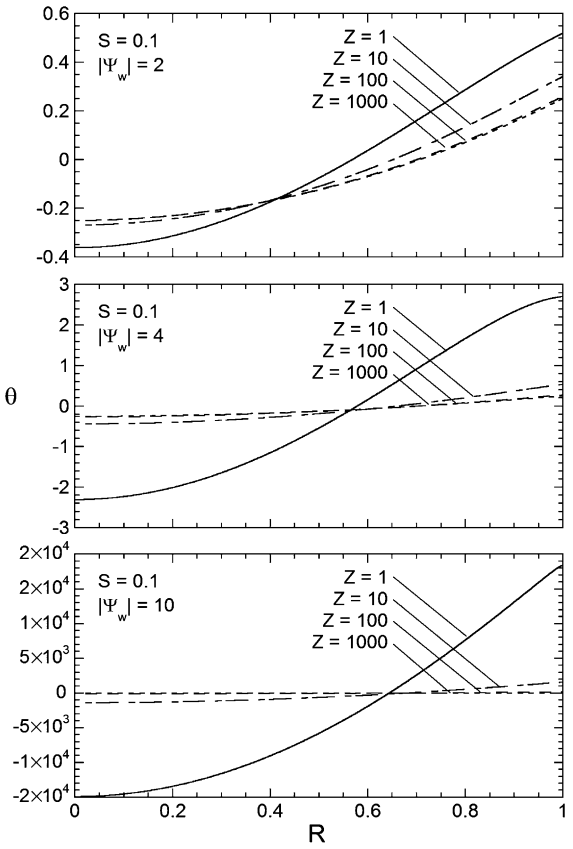

Fig. 9. Radial profiles of dimensionless fluid temperature for three values of $|\Psi_w|$ and $S = 0.1$ for $1 \leqslant Z \leqslant 1000$ for the constant wall heat flux boundary condition.

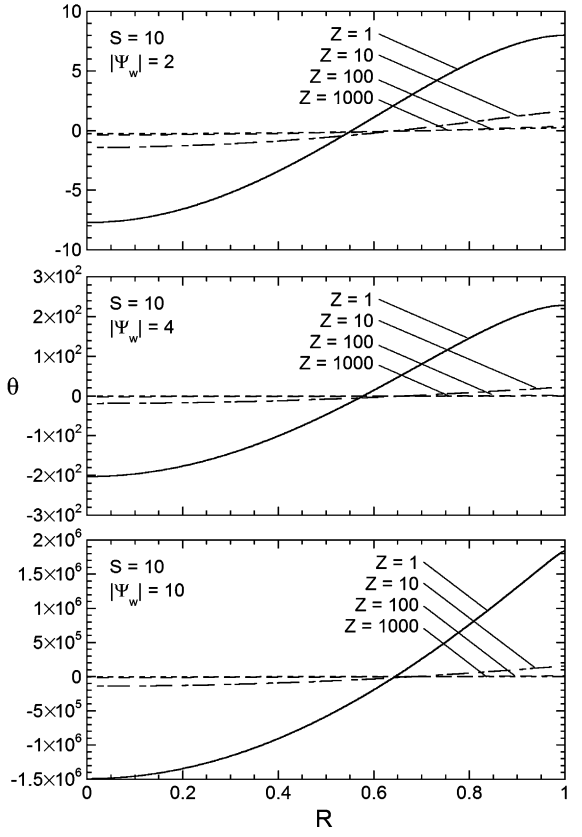

Fig. 10. Radial profiles of dimensionless fluid temperature for three values of $|\Psi_w|$ and $S = 10$ for $1 \leqslant Z \leqslant 1000$ for the constant wall heat flux boundary condition.

the total Joule heating is reduced (see Fig. 6), and thus, θ becomes less dependent on Z and further, is more uniform across the tube. It should be noted that for $|\Psi_w| < 2$ and large values of Z, the dimensionless temperature becomes independent of the Joule heating parameter S, as was reported previously [34]. However, no such limiting behavior exists for high wall potentials.

The variation in fully-developed Nusselt number with $|\Psi_w|$ is illustrated for $1 \leqslant Z \leqslant 1000$ and $0.1 \leqslant S \leqslant 100$ in Fig. 11. The Nusselt number decreases monotonically from its maximum value at $|\Psi_w| \to 0$. For low Z (where the velocity profile is nearly parabolic) and $S \to 0$, $Nu \approx 4.36$, corresponding to the Nusselt number for classical Poiseuille flow in a circular tube in the absence of Joule heating [38]. The maximum Nusselt number is dependent on the electro-kinetic radius Z and the magnitude of the Joule heating parameter S. This maximum increases with increasing Z and decreasing S. At large values of Z (for which the velocity is independent of radius in the tube), the maximum $Nu = 8$ corresponds to the limit of slug flow with vanishing Joule heating, observed for $|\Psi_w| \to 0$ and/or $S \to 0$. The Nusselt number vanishes for both increasing $|\Psi_w|$ and/or increasing S at

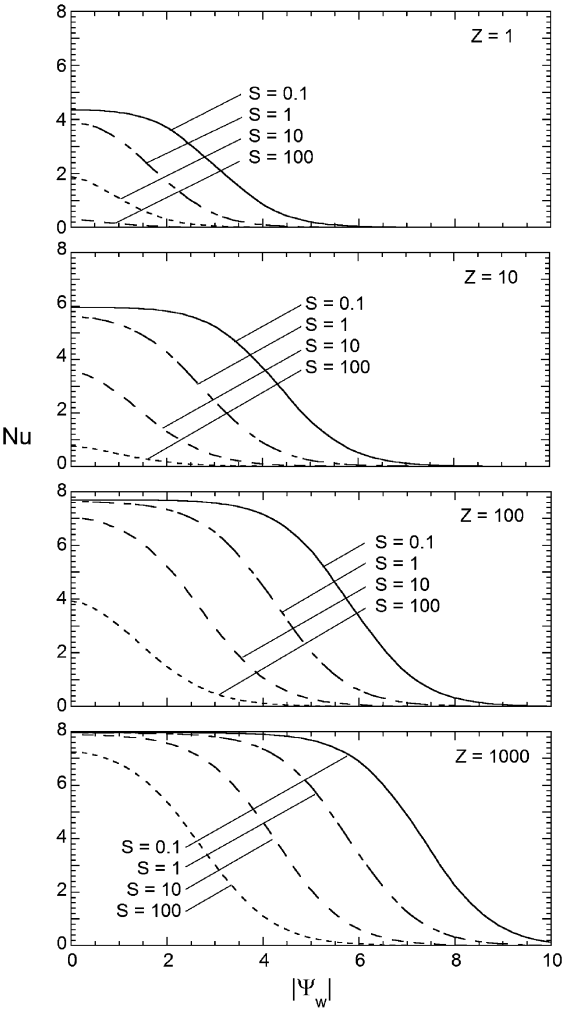

Fig. 11. Variation of the fully-developed Nusselt number with $|\Psi_w|$ for $0.1 \leqslant S \leqslant 100$ and $1 \leqslant Z \leqslant 1000$.

all values of Z, due to the increasingly large dimensionless wall temperature which results from intense Joule heating.

The significant dependence of the Nusselt number on the wall potential is noted in Fig. 11. The magnitude of the dimensionless wall potential in typical electro-osmotic flow applications exceeds $|\Psi_w| \approx 4$. Fig. 11 reveals that predicting the fully-developed Nusselt number (or dimensionless wall temperature) using the low-ζ_w assumption results in values which are seriously in error. The Nusselt number may be over-predicted by several hundred percent and thus, the wall temperature would be substantially under-predicted.

The variation of the fully-developed Nusselt number with Z, S, and $|\Psi_w|$ have been correlated using an expression similar to Eq. (17)

$$Nu = C_4\{\tanh[0.75(|\Psi_w| - C_5)] - 1\} \tag{19}$$

However, in this case the parameters depend in a rather complex way on S and Z. C_4 is described by the following:

$1 \leqslant Z \leqslant 100$:

$$C_4 = -Z^{0.115}\left\{0.23 + \frac{4.36}{[0.72 + S/(10+Z)]^2 + 1.62}\right\} \tag{20a}$$

$100 \leqslant Z \leqslant 1000$:

$$C_4 = -Z^{0.015}\left\{1.81 + \frac{0.29}{[0.94 + S/(10+Z)]^2 + 0.16}\right\} \tag{20b}$$

C_5 takes the following form:

$1 \leqslant Z \leqslant 10$:

$$C_5 = 0.79 + 4.31\exp\left\{-\left[0.19\ln(342.5S/\sqrt{Z})\right]^2\right\} - 0.4/S \tag{21a}$$

$10 \leqslant Z \leqslant 1000$:

$$C_5 = 10.49 - 9.59\exp\left\{-[0.085\ln(0.044S/Z)]^2\right\} \tag{21b}$$

This correlation predicts the Nusselt number to within 3% of the maximum Nusselt number ($Nu_{\max} = 8$) for the range of problem parameters studied here ($1 \leqslant Z \leqslant 1000$, $0.1 \leqslant S \leqslant 100$, and $0 \leqslant |\Psi_w| \leqslant 10$).

4. Conclusions

Fully-developed electro-osmotic flow and heat transfer in a circular tube has been investigated for arbitrary wall zeta potentials for a range of electro-kinetic radius and Joule heating magnitudes. Both constant wall temperature and constant wall heat flux thermal boundary conditions are considered. The coupled differential equations governing charge distribution, and momentum and energy transport were solved numerically. The results clearly show that realistic values of the wall zeta potential produce thermal transport behavior which differs significantly from that predicted by an analysis employing the Debye–Hückel approximation. These differences are manifest primarily in dimensionless temperature profile and Nusselt number, with relatively little effect on the fluid velocity profile. In general, higher values of the wall potential result in temperature distributions characterized by both significantly higher magnitudes and radial gradients. The fully-developed Nusselt number is significantly lower than that predicted by the low-ζ_w analysis. The primary source of deviation occurs due to the highly non-uniform nature of the local volumetric heating which prevails at high wall potential. The results of this study clearly illustrate the error which may be incurred in predicting the thermal transport in electro-osmotic flow assuming low wall potential.

References

[1] R.F. Probstein, Physicochemical Hydrodynamics, second ed., Wiley, New York, 1994.
[2] I.E. Valkó, H. Sirén, M. Riekkola, Characteristics of electro-osmotic flow in capillary electrophoresis in water and in organic solvents without added ionic species, J. Microcolumn Sep. 11 (1999) 199–208.
[3] N.A. Polson, M.A. Hayes, Electro-osmotic flow control of fluids on a capillary electrophoresis microdevice using an applied external voltage, Anal. Chem. 72 (2000) 1088–1092.
[4] C.L. Rice, R. Whitehead, Electrokinetic flow in a narrow cylindrical capillary, J. Phys. Chem. 69 (1965) 4017–4024.
[5] D. Burgreen, F.R. Nakache, Electrokinetic flow in ultrafine capillary slits, J. Phys. Chem. 68 (1964) 1084–1091.
[6] S. Levine, J.R. Marriott, G. Neale, N. Epstein, Theory of electrokinetic flow in fine cylindrical capillaries at high zeta-potentials, J. Colloid Interf. Sci. 52 (1974) 136–149.
[7] Y.J. Kang, C. Yang, X.Y. Huang, Dynamic aspects of electro-osmotic flow in a cylindrical microcapillary, Int. J. Eng. Sci. 40 (2002) 2203–2221.
[8] Y.J. Kang, C. Yang, X.Y. Huang, Electro-osmotic flow in a capillary annulus with high zeta potentials, J. Colloid Sci. 253 (2002) 285–294.
[9] J.P. Hsu, C.Y. Kao, S. Tsent, C.J. Chen, Electrokinetic flow through an elliptical microchannel: Effects of aspect ratio and electrical boundary conditions, J. Colloid Interf. Sci. 248 (2002) 176–184.
[10] C. Yang, D. Li, Electrokinetic effects on pressure-driven liquid flows in rectangular microchannels, J. Colloid Interf. Sci. 194 (1997) 95–107.
[11] D.W. Arnold, P.H. Paul, Fluorescence-based visualization of electro-osmotic flow in microfabricated systems, in: Proceedings of SPIE-The International Society for Optical Engineering, Bellingham, WA, vol. 3877, 1999, pp. 174–179.
[12] P.H. Paul, M.G. Garguilo, D.J. Rakestraw, Imaging of pressure- and electrokinetically-driven flows through open capillaries, Anal. Chem. 70 (1998) 2459–2467.
[13] J.A. Taylor, E.S. Yeung, Imaging of hydrodynamic and electrokinetic flow profiles in capillaries, Anal. Chem. 65 (1993) 2928–2932.
[14] D. Ross, T.J. Johnson, L.E. Locascio, Imaging of electro-osmotic flow in plastic microchannels, Anal. Chem. 73 (2001) 2509–2515.
[15] T. Tsuda, M. Ikedo, Observation of flow profiles in electro-osmosis in a rectangular capillary, J. Chromatogr. 632 (1993) 201–207.
[16] E.B. Cummings, PIV measurement of electro-osmotic and pressure-driven flow components in microfluidic systems, Microelectromechanical Systems (MEMS), MEMS-vol. 1, ASME, 1999, pp. 377–382.
[17] R.J. Yang, L.M. Fu, C.C. Hwang, Electro-osmotic entry flow in a microchannel, J. Colloid Interf. Sci. 244 (2001) 173–179.

[18] S. Arulanandam, D. Li, Liquid transport in rectangular microchannels by electro-osmotic pumping, Colloids Surf. 161 (2000) 29–102.
[19] T.L. Sounart, J.C. Baygents, Electrically-driven fluid motion in channels with streamwise gradients of the electrical conductivity, Colloids Surf. A 195 (2001) 59–75.
[20] L. Ren, D. Li, Electro-osmotic flow in heterogeneous microchannels, J. Colloid Interf. Sci. 243 (2001) 255–261.
[21] J.P. Gleeson, Electro-osmotic flows with random zeta potential, J. Colloid Interf. Sci. 249 (2002) 217–226.
[22] J.G. Santiago, Electro-osmotic flows in microchannels with finite inertial and pressure forces, Anal. Chem. 73 (2001) 2353–2365.
[23] J.H. Knox, Thermal effects and band spreading in capillary electro-separation, Chromatographia 26 (1988) 329–337.
[24] W.A. Gobie, C.F. Ivory, Thermal model of capillary electrophoresis and a method for counteracting thermal band broadening, J. Chromatogr. 516 (1990) 191–210.
[25] J.H. Knox, K.A. McCormack, Temperature effects in capillary electrophoresis. 1. Internal capillary temperature and effect upon performance, Chromatographia 38 (1994) 207–214.
[26] J.H. Knox, K.A. McCormack, Temperature effects in capillary electrophoresis. 2. Some theoretical calculations and predictions, Chromatographia 38 (1994) 215–221.
[27] M.A. Bosse, P. Arce, Role of Joule heating in dispersive mixing effects in electrophoretic cells: Hydrodynamic considerations, Electrophoresis 21 (2000) 1018–1025.
[28] M.A. Bosse, P. Arce, Role of Joule heating in dispersive mixing effects in electrophoretic cells: Convective-diffusive transport aspects, Electrophoresis 21 (2000) 1026–1033.
[29] A.S. Rathore, K.J. Reynolds, L.A. Colon, Joule heating in packed capillaries used in capillary electrochromatography, Electrophoresis 23 (2002) 2918–2928.
[30] G.Y. Tang, C. Yang, J.C. Chai, H.Q. Gong, Joule heating effect on electro-osmotic flow and mass species transport in a microcapillary, Int. J. Heat Mass Transfer 47 (2004) 215–227.
[31] L.N. Tao, On some laminar forced-convection problems, ASME J. Heat Transfer 83 (1961) 466–472.
[32] L.N. Tao, The second fundamental problem in heat transfer of laminar forced convection, J. Appl. Mech. (June) (1962) 415–420.
[33] E.M. Sparrow, J.L. Novotny, S.H. Lin, Laminar flow of a heat-generating fluid in a parallel-plate channel, AIChE J. 9 (1963) 797–804.
[34] D. Maynes, B.W. Webb, Fully developed electro-osmotic heat transfer in microchannels, Int. J. Heat Mass Transfer 46 (2003) 1359–1369.
[35] D. Maynes, B.W. Webb, The effect of viscous dissipation in thermally fully-developed electro-osmotic heat transfer in microchannels, Int. J. Heat Mass Transfer 47 (2004) 987–999.
[36] B.D. Iverson, D. Maynes, B.W. Webb, Thermally developing electro-osmotic convection in rectangular microchannels with vanishing Debye layer thickness, AIAA J. Thermophys. Heat Transfer 18 (2004) 486–493.
[37] Handbook of Chemistry and Physics, CRC Press, Cleveland, Ohio, 1986.
[38] W.M. Kays, M.E. Crawford, Convective Heat and Mass Transfer, third ed., McGraw-Hill, New York, 1993.
[39] S.V. Patankar, Numerical Heat Transfer and Fluid Flow, Hemisphere, New York, 1980.